Journal of Alloys and Compounds 521 (2012) 155–162

Contents lists available at SciVerse ScienceDirect

Journal of Alloys and Compounds

journal homepage: www.elsevier.com/locate/jallcom

Physical properties and heterojunction device demonstration of aluminum-doped ZnO thin films synthesized at room ambient via sol–gel method

Hakan Karaagac*, Emre Yengel, M. Saif Islam

Department of Electrical and Computer Engineering, University of California at Davis, Davis, CA 95616, USA

ARTICLE INFO

Article history:
Received 23 November 2011
Received in revised form 14 January 2012
Accepted 16 January 2012
Available online 30 January 2012

Keywords:
Thin films
Oxide materials
Sol–gel process
X-ray diffraction

ABSTRACT

ZnO and some of its ternary wide-bandgap alloys offer interesting opportunities for designing materials with tunable band gaps, strong piezoresistivity and controlled electrical conductance with high optical transparency. Synthesizing these materials on arbitrary substrates using low-cost and unconventional techniques can help in integrating semiconductors with different physical, electrical, and optical characteristics on a single substrate for heterogeneous integration of multifunctional devices. Here we report the successful synthesis of aluminum (Al) doped ZnO (AZO) thin films on soda-lime glass, silicon and fluorine doped tin oxide (FTO) pre-coated glass substrates by using sol–gel deposition method at ambient condition. X-ray diffraction (XRD) analysis revealed that varying degree of Al doping significantly impacts the crystal orientation, semiconductor bandgap and optical transparency of the film. Crystal structure of the film is also found to be strongly correlated to the characteristics of the substrate material. The impact of heating rate during post annealing process is studied and optimized in order to improve the surface morphology of the deposited films. Optical characterizations have revealed that bandgap energy of AZO films can be tuned between 3.30 eV and 4.1 eV as the Al concentration is varied from 1% to 20%. Similarly, electrical characteristics of these films indicate that 1% AZO film has the lowest resistivity of 2.2×10^{-2} Ω cm. Finally, 1% Al doped AZO thin film was used in fabricating a p-Si/n-AZO heterojunction, which exhibited good diode characteristics with more than five orders of magnitude rectification ratio and an ideality factor of 3.28.

© 2012 Elsevier B.V. All rights reserved.

1. Introduction

Recently, ZnO, a well-known II–VI semiconductor with a large band gap (3.37 eV) and exciton binding energy (60 meV) at room temperature, has drawn significant interest due to its unique properties such as high thermal stability, near band emission, piezoelectricity, transparent conductivity, natural abundance and non-toxic nature [1–7]. These properties make ZnO a potential candidate for various applications, such as optoelectronic devices, chem-bio and gas sensors, solar cells, field emission devices transistors, hydrogen storage and lasers operating at room temperature [2,8]. It is intrinsically an n-type semiconductor origin of which is still under investigation. Recent studies have shown that hydrogen and some kind of native defects, such as zinc interstitials and oxygen vacancies, are involved in the n-type conductivity of ZnO [9].

Although considerable efforts have been made to achieve p-type conductivity in ZnO, which is essential for the fabrication of efficient p–n homojunctions, the realization of re-producible high quality p-type ZnO is still challenging. For the construction of ZnO based opto-electronic devices, it is therefore essential to find alternative approaches for the fabrication of ZnO heterojunctions with appropriate materials. The ZnO based heterojunctions are usually fabricated by depositing n-ZnO on diverse p-type materials, such as GaN, Si, different polymers and some organic compounds [10–13]. Among these materials, Si is one of the most appropriate candidates in the realization of cost-effective ZnO based opto-electronic devices not only due to its low cost and high crystal quality but also its highly developed micro-electronic technology. Therefore, there are already many studies reported in literature on n-ZnO/p-Si due to its simple structure and providing unique properties [14–21].

Despite intrinsically being a high resistive material, conductive ZnO can be fabricated by doping with appropriate metal species such as Al, Ga, Sn, Cd, and In. Among them, Al doped ZnO (AZO) can be employed as a potential alternative to well-known transparent conductive oxides such as indium tin oxide (ITO), which is unattractive due to high cost and limited supply of indium. Because of being a low-cost and earth-abundant element, Al is an ideal candidate to replace indium (In). AZO is one of the most promising compounds in terms of high visible transparency, good electrical conductivity, high chemical and mechanical stability [22]. So far, various fabrication techniques reported including direct current (DC)/radio

* Corresponding author.
E-mail address: hkaraagac@ucdavis.edu (H. Karaagac).

0925-8388/$ – see front matter © 2012 Elsevier B.V. All rights reserved.
doi:10.1016/j.jallcom.2012.01.103

frequency (RF) sputtering, reactive evaporation, spray pyrolysis, MOCVD and sol–gel process [23–29]. Among them, sol–gel offers significant advantages in terms of precise compositional control and good homogeneity [30].

In this work, undoped and Al doped ZnO thin films were deposited on glass, silicon and FTO coated glass substrates by using sol–gel process at ambient condition. To investigate the impact of Al doping on electrical and optical properties of AZO thin film, ZnO was doped with different Al doping concentrations. Finally, as an application, AZO thin film was deposited on p-type Si wafer, for the construction of n-AZO/p-Si heterojunction.

2. Experimental details

Undoped ZnO precursor solution was prepared by dissolving zinc acetate dihydrade (ZnAc:Zn$(COOCH_3)_2\cdot2H_2O$] in 2-proponal and diethanolamine (DEA, $C_4H_{11}NO_2$), which were used as solute, solvent and chelating agent, respectively. ZnAc was first dissolved in 2-proponal and followed by addition of DEA to increase the solubility and deionized (DI) water to prevent the precipitation of solution. The molar ratio of DEA/ZnAc and H2O/ZnAc were chosen as 1 and 1/2, respectively corresponding to a solution with 0.4 M concentration, as reported elsewhere [31]. In addition, to prepare Al doped ZnO (AZO) precursor solution, aluminum nitrate [$Al(NO_3\cdot9H_2O)$ was used as doping agent. To obtain AZO thin films with different Al doping concentrations, solutions with different Al/Zn molar ratios, varied between 1 and 20, were prepared by adding aluminum nitrate to the precursor solution prepared for ZnO. The prepared precursor solutions were stirred at 70 °C for 1 h to yield a clear and homogenous solution. During the spin coating process, 0.45 μm WHATMAN syringe filters were used for filtering pre-cursor solution. Thin films were deposited on different pre-cleaned substrates (soda-lime glass, Si and fluorine doped thin oxide (FTO) coated glass) by spin coating at one step with spinning speed of 5000 revolutions per minute (rpm) for 1 min. The spin coating process was repeated two times for both undoped and Al doped ZnO thin films to obtain 250 nm thick films (measured by a Dektak 3030 profilometer). In order to remove organic species in thin film structure, films were first pre-heated at 300 °C on hot plate for 5 min and then it was followed by annealing at 550 °C for 1 h in air ambient for complete crystallization of the thin film and evaporation of the remaining organics in the structure.

The crystal structure and orientation, existing material phases and the size of the grains were determined by means of X-ray diffraction (XRD) using a Scintag XDS2000 powder X-ray diffractometer with Cu Kα radiation source. The measurements were taken in the range of 25–60 °C with a scan speed of 2°/min. The surface morphology and thickness of deposited thin films were determined by a Hitachi S-4100 FE scanning electron microscopy (SEM). The optical properties were characterized by performing transmission measurements in the wavelength range of 300–1100 nm using an Ocean Optics UV–vis spectrometer. To investigate the electrical properties of the films, resistivity measurements were carried out on samples having van der Pauw contact geometry at room temperature (300 K). Front and back ohmic contacts of n-AZO/p-Si device were achieved by electron-beam (E-beam) evaporation of Al through copper shadow masks followed by annealing at 350 °C under N_2 gas flow to ensure good ohmic contacts. The dark current (*I*)–voltage (*V*) characteristics of the devices were measured at room temperature using a HP 4156B semiconductor parameter analyzer. Finally, a Sunray 400 SM UV (Uvitron International) light sources was used for the measurement of *I–V* characteristics of deposited film and fabricated heterojunction under UV-illumination.

3. Results and discussion

3.1. X-ray diffraction analysis

Fig. 1(a) shows the X-ray diffraction (XRD) patterns obtained for an undoped ZnO thin film deposited on a soda-lime glass substrate. As can be seen from the figure, there are diffraction peaks discernable in the spectrum at 2θ position of 31.92, 34.56, 36.42, 47.76 and 56.80 corresponding to (1 0 0), (0 0 2), (1 0 1), (1 0 2) and (1 1 0), respectively, which belong to a hexagonal crystal structure with lattice parameters of $a = 3.249$ Å and $c = 5.206$ Å [32]. As can be seen clearly from the inset of Fig. 1(a), showing the (1 0 1) and (0 0 2) peaks in magnified scale following the smoothing and background elimination, it appears that the (0 0 2) peak dominates the pattern, indicating the prevailing direction of orientation during thin film growth. Fig. 1(b) presents the XRD patterns obtained for a 5% Al doped ZnO (AZO) thin film. It shows that AZO thin film is crystalline and exhibits the same crystal structure as detected for an

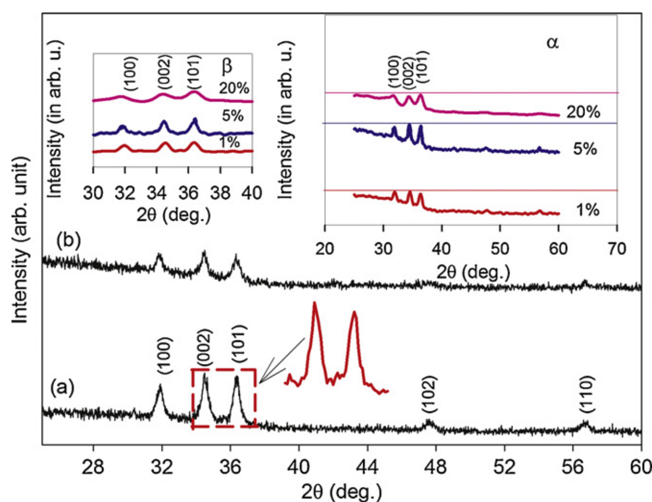

Fig. 1. (a) X-ray diffraction (XRD) pattern obtained for undoped ZnO thin film. Diffraction peaks discernable in the spectrum reveals the formation of polycrystalline ZnO structure and the (0 0 2)-orientation is the prevailing direction of the thin film growth. Inset figure shows the (1 0 1) and (0 0 2) peaks in magnified scale following the smoothing and background elimination. (b) XRD pattern obtained for 5% Al doped ZnO thin film. Following the Al doping the variation in intensity for all peaks indicates the structural modifications are taking place during doping process. Inset figures labeled by α and β show the obtained XRD patterns for 1%, 5% and 20% Al doped ZnO thin films following the smoothing and background elimination processes, respectively.

undoped ZnO film, which can be seen from the existence of diffraction peaks and their position with respect to those defined for ZnO, respectively. However, as can be seen in Fig. 1(b), subsequent to Al doping (5%), there is a decrease in intensity for all the reflecting planes, which suggests that structural reorganization and modifications are taking place during the doping process. In general, the decrease in the intensity and the broadening of the full width at half maximum (FWHM) of the peaks can be explained by the existence of deterioration of crystallinity.

The incorporation of Al in the place of Zn may give rise to the generation of different sorts of stress stemming from the differences in the ion size between Al and Zn, which could be the reason behind the modifications observed in the structure [33]. In addition, the XRD patterns obtained for 1%, 5% and 20% Al doped ZnO thin films are presented as inset in Fig. 1(b). Inset figures labeled by α and β show the obtained XRD patterns for Al doped ZnO thin films following the smoothing and background elimination processes, respectively. It is clear from these figures that although the peak intensities of (0 0 2) and (1 0 1) are comparable for 1% Al doped sample, the intensity of (1 0 1) starts to dominate in the structure with further increase in Al doping concentration. The variation in the (1 0 1) orientation subsequent to Al doping is closely related to the change in the nucleation process and the chemical conditions during the synthesis process [34]. The impact of Al doping on crystal orientation of ZnO thin film has been extensively reported in literature, which is consistent with the results observed in this study [35].

It is important to notice that neither Al_2O_3 nor Al phase were found to appear in the XRD pattern after the doping process, which might be due to the Al substituting the Zn in the lattice, as was reported elsewhere [36]. To understand the impact of the substrate materials on the crystal quality of the thin film, ZnO doped with 1% Al (AZO) was deposited on various substrates, including soda-lime glass, p-Si and fluorine doped tin oxide (FTO) pre-coated glass substrates. Recorded XRD patterns for the AZO films deposited on these materials are depicted in Fig. 2(a). Based on these patterns, it is observed that all films are crystalline with hexagonal system and substrate material has a significant influence on the crystal quality

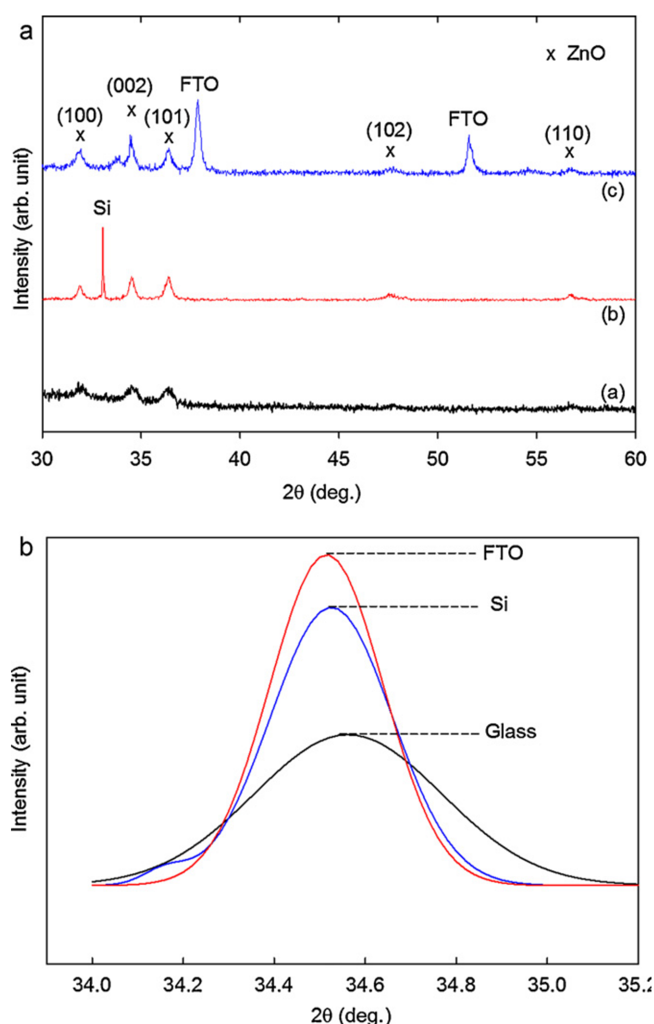

Fig. 2. (a) The X-ray diffraction (XRD) patterns recorded for 1% Al doped ZnO (AZO) thin film deposited (a_a) glass, (a_b) p-Si, (a_c) FTO pre-coated glass substrates. (b) The comparison of full width at half maximum (FWHM) and intensity of (0 0 2) peak obtained for AZO thin film deposited on these substrates.

of deposited film. The crystallinity gradually improves for the films deposited on soda-lime glass, Si and FTO coated substrates. In other words, the best crystal quality is obtained for the film deposited on FTO coated substrate, which could be seen from the smaller FWHM and higher intensity of (0 0 2) peak as shown in Fig. 2(b) and Table 1.

In fact, there are various potential factors behind the influence of the substrate materials on the crystallinity including substrate roughness and stoichiometry, mismatch in thermal expansion coefficient and lattice parameters. In this regard, the better crystallinity obtained for the film on FTO is quite reasonable due to the similarity of the structures of FTO and AZO. Otherwise, the lattice-mismatch between them may induce different magnitude of stress which triggers the formation of disorder throughout the crystal structure resulting in an increase in the density of grain boundaries [37].

Table 1
Calculated parameters of (0 0 2) reflecting planes in the crystal structure of 1% Al doped ZnO thin films.

Sample	2θ (in°)	FWHM (in°)	Intensity	Grain size (D) (nm)
AZO on glass	34.56	0.4863	87	18
AZO on Si	34.52	0.3153	160	26
AZO on FTO	34.51	0.2929	190	30

Grain size calculations for AZO thin film deposited on glass, Si and FTO were carried out using Schrerrer's equation [38]

$$D = \frac{0.89\lambda}{\beta \cos\theta} \quad (1)$$

where λ, β and θ are X-ray wavelength, FWHM of θ and Bragg diffraction angle, respectively. The calculations were carried out based on (0 0 2) peak following the background elimination and smoothing process as shown in Fig. 2(b). The obtained grain size (D), FWHM, θ and intensity are presented in Table 1. The results revealed that largest grains (30 nm) were formed in the structure of AZO thin film deposited on the FTO substrate, indicating that the best crystal quality achieved with FTO compared to glass and Si substrates.

3.2. *Surface morphology analysis of thin films*

The surface morphology of undoped ZnO thin film deposited on glass substrate is shown in Fig. 3(a and b). As can be seen from Fig. 3(a), wrinkle like pattern has formed on the surface of sol–gel thin film. The growth technique, condition and parameters may have profound effect on the morphology of a deposited thin film. As mentioned earlier, during the growth via the sol–gel process, following each spin coating step, the deposited layer was pre-heated at 300 °C for 5 min to evaporate the solvent and organics species, followed by an annealing at 550 °C for 1 h subsequent to the completion of all thin spin-coated layers to improve the crystallization of thin film. To understand the basic mechanism behind the wrinkle formation, different heating rates were applied to films while they were annealed at 550 °C. According to Fig. 3(c and d), these formations appeared only for films annealed with high heat ramp-up rate (40 °C/min), and it was not the case for slow heating rates below (9 °C/min).

The wrinkle formation in the sol–gel derived ZnO thin film was reported elsewhere [39] and it was attributed to the relaxation of stress as a consequence of the evaporation of solvent during drying process by which the skeletal branches like pattern formation was observed on the surface of ZnO thin film. In our case, since no wrinkle of any kind was observed at low heating rate, it is reasonable to suggest that during the annealing process, the evaporation rate of the liquid in the sol–gel matrix of deposited film induces different sorts of stress which leads to the formation of wrinkles. In other words, shrinkage of a gel takes place as liquid evaporates which subsequently leads to the deformation of the film and forms a network consisting of liquid and solid phases. Moreover, during drying process, as the thermal expansion coefficient of substrate and deposited ZnO is different, the fast heating rate may result in a compressive stress which may cause bending in the gelated film [39]. It is also clear from Fig. 3(b) that there is an inhomogeneous wrinkle pattern distributed over the complete surface of ZnO thin film, which could be due to the differences between the evaporation of the solvent at different parts of the sample during heating process. To validate our postulate about the impact of the heating rate on the wrinkle formation, 1% Al doped ZnO film was also examined by heating with different rates during the annealing stage. It was found that films annealed with low heating increments had a very smooth surface without any wrinkle or wavy patterns as shown in Fig. 3(d).

3.3. *Optical characterization of thin films*

Optical transmittance measurements were carried out for both undoped and Al doped ZnO thin films with different concentrations deposited onto soda-lime glass substrate at room temperature. Fig. 4(a–d) shows the spectral distribution of transmittance for these films in the wavelength range of 300–950 nm. Both undoped

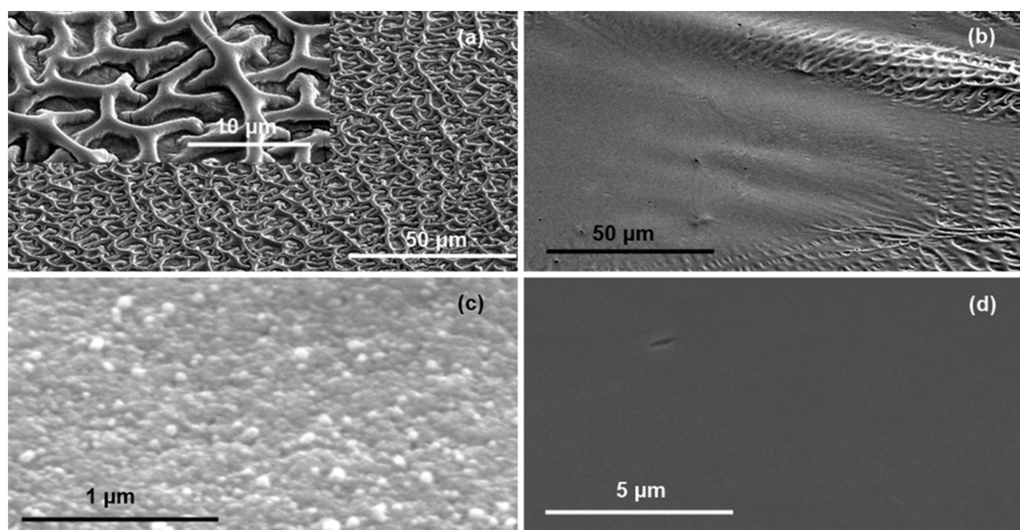

Fig. 3. Scanning electron microscopy (SEM) imaging of ZnO and Al:ZnO (AZO) thin films deposited on glass substrate. (a) SEM image shows the wrinkle pattern formation on the surface of ZnO thin film following the annealing at 550 °C with high ramp-up rate. (b) Micrograph is revealing the inhomogeneous wrinkle pattern distribution over the surface of film. (c) SEM image that indicates surface morphology of film annealed at 550 °C with low ramp-up rate. (d) Image shows the surface morphology of AZO (1% Al doped ZnO) thin film after annealed at 550 °C with low ramp-up rate.

and Al doped ZnO films have high transparency in the visible range. The transmittance of undoped and 20, 5 and 1% Al doped ZnO thin films in the wavelength range of 400–900 nm is found in between 90 and 100, 70 and 80, 80 and 100 and 95 and 100%, respectively. These observations indicate that there is a decrease in transparency as the Al doping concentration increases from 1 to 20%. Although there may be different potential factors that impact the transparency of the films, the major factor is probably the bulk and surface scattering centers formed as a consequence of Al diffusion mechanism in the polycrystalline structure up on exceeding the maximum solubility of Al in the ZnO film matrix.

When the Al doping reaches beyond the solubility limit, Al atoms cannot occupy the place of Zn in the lattice. Instead, neutral Al atoms either accumulate at the grain boundaries or segregate on the surface of the film which may act as bulk and surface light scattering centers, respectively. These are responsible for the observed reduction in the transparency following the doping process. Beside light scatterings, the incorporation of excess Al may generate disorder

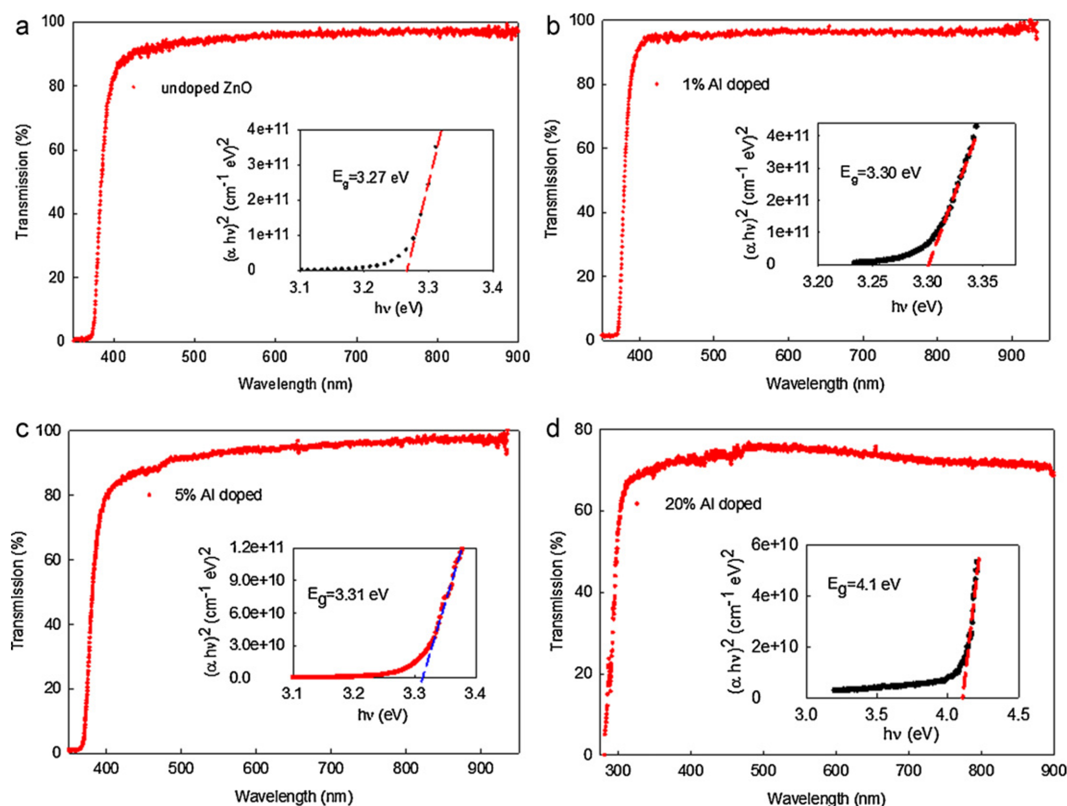

Fig. 4. Optical transmittance spectra obtained for (a) undoped, (b) 1%, (c) 5% and (d) 20% Al doped ZnO thin films. Inset figures show the plot of $(\alpha h\nu)^2$ vs $(h\nu)$ for each film.

in the crystal structure which significantly reduces the amount of light that can pass through the crystal structure.

In order to estimate the optical band gap energy, the relation between the absorption coefficient (α) and photon energy ($h\nu$) was studied by plotting $(\alpha h\nu)^2$ vs ($h\nu$) as shown in the insets of Fig. 4(a–d). From the obtained spectral distribution of transmission, the absorption coefficient was estimated by using

$$\alpha = \frac{1}{d}\ln\left(\frac{I_o}{I}\right) \quad (2)$$

where d, I and I_o are thickness of specimen, intensity of transmitted and incident light, respectively. In addition to the absorption coefficient, the optical band gap energy (E_g) and its nature of it (direct or indirect) can be determined through

$$(\alpha h\nu) = A(h\nu - E_g)^n \quad (3)$$

where A is a constant which depends on refractive index of the material and n is an exponent index determining the type of transition in the band gap. The value of $n = 1/2$ and 2 corresponds to the existence of direct and indirect band gap, respectively [40]. The optical band gap is evaluated through the $(\alpha h\nu)^2$ vs ($h\nu$) relation by extrapolating the linear region of the curves on the energy axis ($(\alpha h\nu)^2 = 0$). The obtained curves of $(\alpha h\nu)^2$ vs ($h\nu$) are linear for $n = 1/2$, indicating a direct band gap nature for both undoped and Al doped ZnO thin films. Fig. 4(a–d) shows that the absorption onset is shifted to shorter wavelengths (blue shift) as the Al doping concentration increases, called the band gap enhancement. The optical band gaps were calculated as 3.27 and 3.30, 3.31 and 4.10 eV for undoped and 1, 5 and 20% Al doped ZnO thin films, respectively as given in Fig. 5.

Researchers have reported different band gap energy values for ZnO thin films grown using various methods. In general, these values range between 3.20 and 3.32 eV [41], which is consisted with the values we obtained for our ZnO thin film. On the other hand, it can be seen from Fig. 5 that the band gap energy value systematically increases as the Al doping concentration increased between 1 and 20% in this study. Although the average crystallite size, internal stress and free carrier concentration have a significant effect on determining energy band gap of a material, the broadening of band gap with the increase of doping concentration is generally explained by Burstein–Moss shift [42]. According to Burstein–Moss shift, heavy doping leads to occupied states at the bottom of conduction band and since a basic principle of quantum mechanics (Pauli principle) prevents the energy states in this region being doubly occupied, the electrons generated by photons from valance band has to excite to higher energy levels in the conduction band which corresponds to the band gap enhancement. Therefore, the observed band gap shift of ZnO thin film from 3.31 to 4.1 eV on increasing Al doping concentration from 1 to 20% is probably stemming from this effect. A similar variation in the bandgap for the heavily doped ZnO thin film with Al was reported by Di Trolio et al. [43], which was also attributed to Burstein–Moss shift.

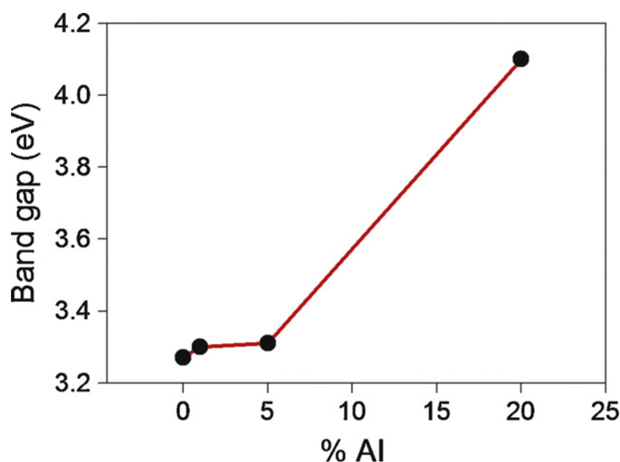

Fig. 5. Variation of optic band gap as a function Al doping concentration. Band gap shift is observed on increasing Al concentration from 1 to 20, explained by Burstein–Moss effect.

3.4. Electrical characterization of thin films

Fig. 6 shows the room temperature I–V characteristics of undoped and Al doped ZnO thin films grown on soda-lime glass substrate, which is measured at room temperature. In all these films, Al contacts exhibit ohmic behavior, indicating that the deposited Al contacts by E-beam in van der Pauw contact geometry can be used for the resistivity measurements. The I–V characteristics of ZnO thin film before and after Al doping significantly change in terms of obtained current for a given specific voltage value. On doping ZnO with 20% Al, it was observed that the measured current was lower than that obtained for undoped ZnO. A gradual increase in the current is observed with decreasing Al doping concentration up to 1% concentration. The resistivity of both undoped and Al doped ZnO thin films were determined by applying conductivity measurements to samples with van der Pauw contact geometry at

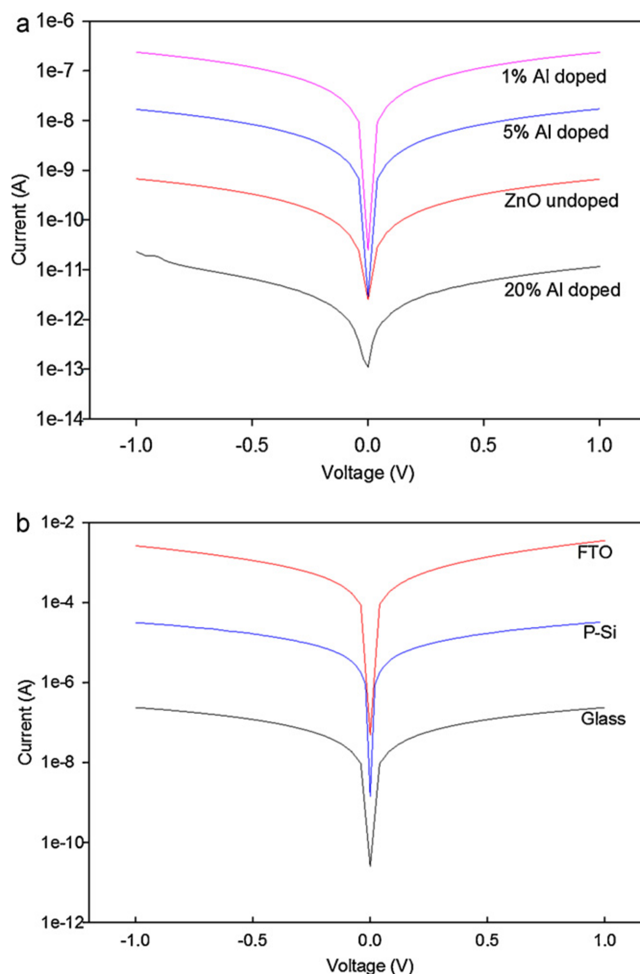

Fig. 6. (a) I–V curves obtained for undoped and Al doped ZnO (AZO) thin films in dark condition which show a systematic decrease in resistivity as Al concentration decreases from 20 to 1%. (b) I–V curves recorded for AZO thin film deposited on glass, silicon and FTO pre-coated glass substrates under dark condition, which reveal that the highest current is obtained for AZO film deposited FTO and followed by those on Si and glass at a given constant voltage.

Table 2
Calculated electrical resistivity of undoped and Al doped ZnO thin films at room temperature.

Sample	Resistivity (Ω cm)
Undoped	1.6×10^5
20% Al	4.9×10^6
5% Al	6.6×10^3
1% Al	4.7×10^2

room temperature. The calculated values are given in Table 2. It is found that undoped ZnO exhibits high resistivity and Al doping has a remarkable effect on the resistivity of the thin films. The resistivity of 20% Al doped film is higher than that obtained for undoped and it systematically reduces with decreasing doping concentration from 20 to 1%. The lowest resistivity is obtained for thin film doped with 1% Al, 470 (Ω cm). The capability of decreasing the resistivity of ZnO by Al doping is a very practiced approach, which is based on the incorporation of Al into the lattice structure of ZnO in place of Zn atoms by which more donor levels are generated, given that ZnO exhibits intrinsic n-type conductivity.

The more incorporation of Al atoms in place of Zn leads to generation of more free electron that can contribute to current which subsequently reduces the resistivity of ZnO thin film. However, in the case of heavily doping, the concentration of Al exceeds the solubility limit in the ZnO structure and an opposite variation tendency in resistivity is observed since the excess Al atoms cannot replace Zn sites but act as either interstitials in crystal lattice or agglomerated as complex formations at grain boundaries of polycrystalline structure of ZnO thin film. These result in generation of different forms of defects and disorder in crystal structure which act as either trapping (or recombination) or scattering (bulk or surface) centers and subsequently result in a decrease in density or reduce in mobility of free carriers, contributing to the observed increase in the resistivity. Al doping with 1% concentration is found to be the nominal ratio in terms of resistivity in the studied range and above 20% Al doping concentration the resistivity of ZnO thin film start to increase significantly.

In order to investigate the effect of substrate material on electrical properties of 1% Al doped ZnO thin film (AZO), it was deposited on various substrates including soda-lime glass, Si, and FTO pre-coated glass substrates. Fig. 6(b) shows the *I–V* characteristics of AZO film measured at room temperature. It is clear from the *I–V* characteristic that for both reverse and forward bias Al contacts exhibit ohmic behavior. Besides, the measured current at a given voltage systematically changes by changing substrate on which AZO thin film is deposited. The highest current was obtained for film deposited on FTO coated glass and followed by those on Si and glass substrates. The room temperature resistivity of AZO thin film deposited on glass, Si and FTO was found as 4.7×10^2, 3.0 and 2.2×10^{-2} (Ω cm), respectively. The observed significant decrease in resistivity for the film deposited on FTO could be attributed to the lattice-matching between AZO and FTO, which have almost similar crystal structures. The lattice matching condition is not met for the films deposited on glass and Si substrates, which possess significantly different phase of crystallinity and crystal structure. A large lattice-mismatch is expected particularly for the film on glass due to its amorphous structure. As interaction between the adsorbed and substrate atoms determines the type of nucleated centers, the lattice mismatch has a significant influence on the quality of grown film. Large mismatch between two materials may induce different kinds of disorder that acts as either local potential wells or scattering centers. These may result in either a decrease in number or reduction in mobility of generated free carriers. Therefore, the observed relatively high conductive AZO thin film on FTO substrate could be attributed to the close lattice matching, which fairly prevents the generation of such defects in the crystal structure. The better crystallinity of AZO film was confirmed by XRD study as well, which supports the results of the resistivity measurements.

The *I–V* characteristic of ZnO and AZO thin films with different doping concentrations ranging from 1 to 20%, deposited on glass substrate, in dark and under UV-illumination condition is shown in Fig. 7(a–d). As evident from the figure, for all the films, the measured

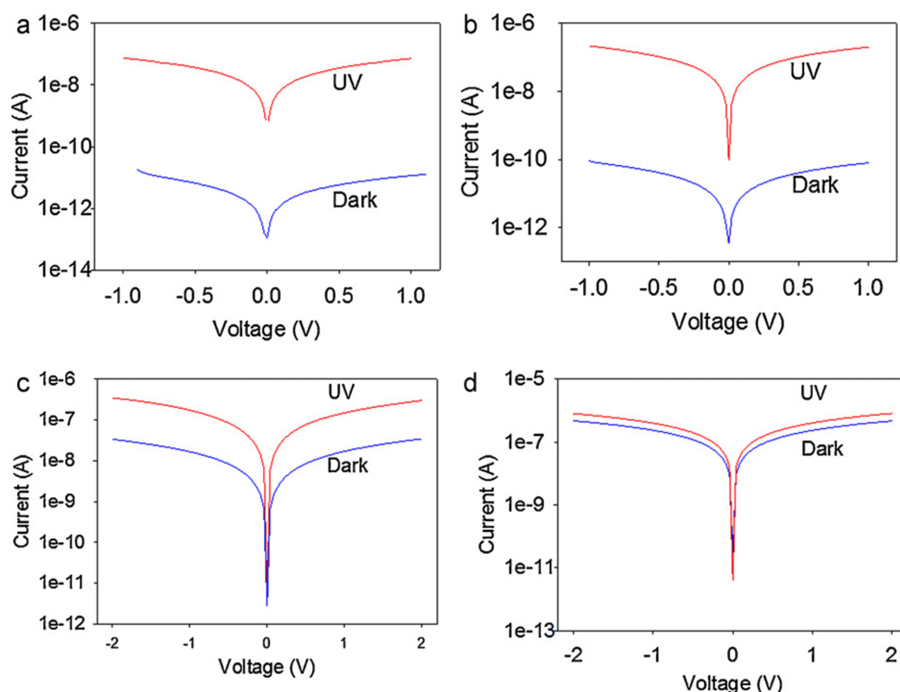

Fig. 7. *I–V* characteristics of (a) 20%, (b) undoped, (c) 5% and (d) 1% Al doped ZnO thin film recorded under both dark and UV-illumination conditions. For all films, there is an increase in current on exposure to UV-light with respect to that measured under dark condition. In addition, figures show the gradual decrease in current under UV-light when film is getting more conductive on decreasing Al doping concentration from 20 to 1%.

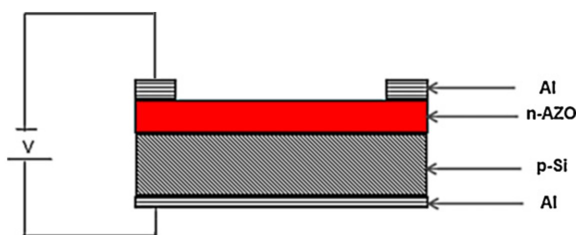

Fig. 8. Schematic representation of n-AZO/p-Si device structure.

currents at a given voltage under UV-illumination condition are higher than those obtained in dark, indicating that more free electron-hole pairs are generated on exposure of films to UV-light. This is important for various applications including UV-detectors and solar cells. It was also evident that UV-sensitivity gradually reduces as film becomes more conductive under dark condition, which is due to the existence of more free carriers in thermal equilibrium relatively with respect to number generated during exposure to UV-light. It is not the case, however, for the highly resistive films as the number of UV-light generated free carriers is either comparable or higher than those in dark condition.

As an application of the deposited AZO thin film, n-AZO/p-Si heterojunction have been fabricated by depositing AZO (1% Al doped ZnO) thin film on pre-cleaned p-Si (1 1 1) wafer with resistivity around 10 (Ω cm), as depicted in Fig. 8. AZO thin film exhibited n-type conduction characteristic, which was verified by hot-probe method. Ohmic front and back electrodes to n-AZO/p-Si device were formed by deposition of Al using E-beam technique. This was followed by device annealing at 350 °C for 30 min under N_2 gas flow to ensure ohmicity of contacts. The diode behavior of hetero-junction was verified by applying voltage and measuring current at room temperature.

The obtained *I–V* characteristic in dark condition is shown in Fig. 9. It can be seen that AZO/Si heterojunction exhibits a perfect diode behavior with rectification factor of 10^5, which is the ratio of forward to reverse current defined by I_f/I_r. The diode parameters including reverse saturation current, ideality factor and series resistance were obtained through the analysis of forward biased *I–V* characteristic. From the semi-logarithmic characteristic of *I–V* for forward bias, the ideality factor (n) can be estimated by using the standard diode equation

$$I = I_s \left[\exp\left(\frac{qV}{nk_BT} \right) - 1 \right] \quad (4)$$

where q, V, k_B, I_s and T are the electronic charge, applied voltage, the Boltzmann constant, saturation current and absolute temperature, respectively [44]. To express the ideality factor parameter explicitly Eq. (4) can be re-written as

$$n = \frac{q}{k_BT} \frac{dV}{d\ \ln I} \quad (5)$$

which clearly imply that n can be evaluated by means of the slope of linear region in curve of semi-logarithmic scale of *I–V* characteristic plotted for the forward bias, as shown in Fig. 9(b). The ideality factor is a diode parameter describing the deviation of a diode from an ideal p–n junction. For the n-AZO/p-Si heterojunction, the ideality factor and saturation current were estimated as 3.28 (for $V < 1$) and 1.86×10^{-9} A, respectively. As known, for the ideal p–n junction, $n = 1$ indicates that there is only pure thermionic emission, while $n > 1$ suggests the existence of different kinds of transport mechanisms that contribute to the carrier transport across the junction [45]. In a similar way, the deviation of n from ideal value for ZnO/Si heterojunction was reported by He et al. [46], which was attributed to the presence of non-linear metal–semiconductor contacts such as metal/Si (Schottky diode) and metal/ZnO (Schottky diode) at specific bias ranges, which give rise to fabrication of 3 different diodes connected in the same structure (metal/n-ZnO/p-Si/metal). Accordingly, the high n value was ascribed to the addition of ideality factors of individual rectifying junctions. Beside that, the high ideality factor was reported for GaN based diodes as well, which was attributed to deep-level-assisted tunneling across p–n junction [47].

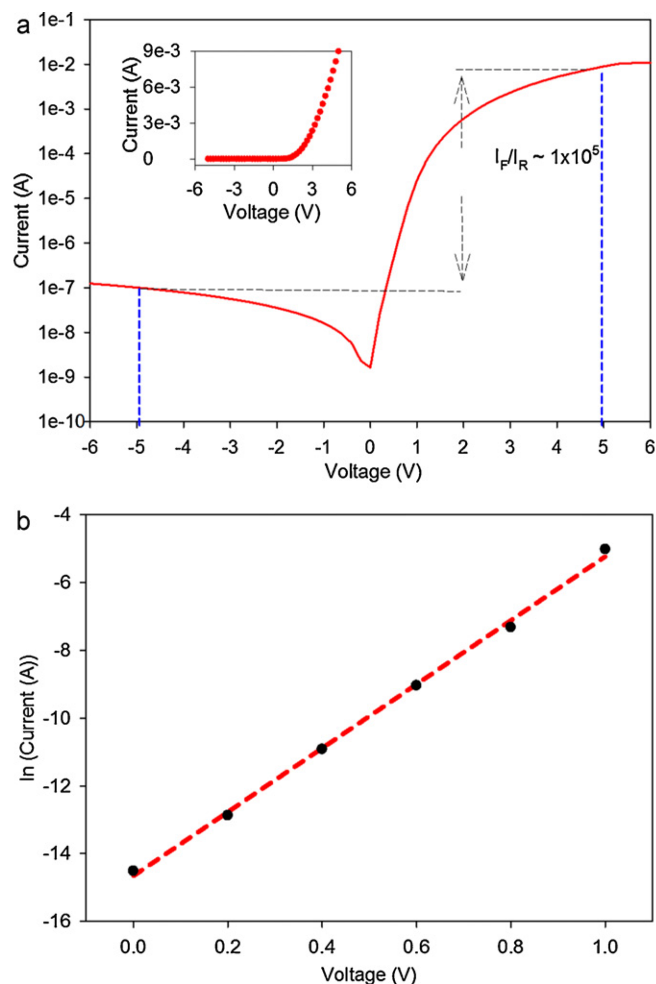

Fig. 9. (a) *I–V* characteristic of n-AZO/p-Si heterojunction under dark condition which shows a perfect diode behavior with rectification factor (I_f/I_r) of 10^5. And, inset figure shows the *I–V* variation in linear scale. (b) Variation of current as a function of forward applied voltage in semi-log scale by which ideality factor (n) can be extracted.

As depicted in Fig. 9(b), the *I–V* curve deviates from the exponential behavior at high voltages. In general, this behavior is attributed to the effect of a series resistance. The standard diode equation in the presence of series resistance can be expressed as

$$I = I_s \left[\exp\left(\frac{q(V - IR_s)}{nk_BT} \right) - 1 \right] \quad (6)$$

and can be used to linearize the experimentally obtained *I–V* characteristic [48]. The series resistance of n-AZO/p-Si junction was found as 370 Ω, nearly one order higher (28 Ω) than reported value for the similar structure [49]. Although high series resistance can originate from different factors, the oxidation of Si substrate before the deposition of AZO thin film and the quality of deposited AZO thin film in terms of crystallinity have major effect on determining the series resistance.

4. Conclusions

Undoped and Al doped ZnO (AZO) thin films were successfully prepared using sol–gel technique. Structural analysis based on XRD measurement has revealed that both ZnO and AZO have the same crystal structures which belong to hexagonal wurtzite system. In addition, it is observed that Al doping has a significant influence on preferential orientation during the fabrication process and promotes the growth in (0 0 2) orientation. XRD study has also shown that AZO thin film with best crystal quality is grown on FTO precoated glass substrate, which is attributed to close lattice matching between AZO and FTO. For the investigation of surface morphology of deposited films, SEM measurements have been carried out for both ZnO and AZO thin films. Based on recorded SEM images, it has been observed that wrinkles forms on the surface of films when annealed with a fast heat ramp up rate. Transmission measurement results have shown that both ZnO and AZO thin films have an average transmittance over 90% for the 400–900 nm range and gradually decreases with increasing Al doping concentration. The optical band gap energy of thin film is evaluated based on transmission spectra and it is found that the band gap energy increases with increasing Al doping concentration, which is explained by Burstein–Moss shift. The effect of Al doping on the resistivity of the ZnO thin film is studied by conductivity measurement performed at room temperature. It is observed that the resistivity gradually decreases with increasing Al doping concentration. The lowest resistivity is observed for 1% Al ZnO thin film, which is 2.2×10^{-2} (Ω cm). Finally, an n-AZO/p-Si heterojunction was fabricated for 1% Al doped AZO thin film and its diode characteristic was determined. Based on measured *I–V* characteristic in dark condition, a perfect rectification factor (10^5) is observed, which indicates the formation of a high quality diode. The demonstrated method of controlled growth of transparent AZO film and heterojunction at ambient condition offers exciting opportunities for designing single-crystal devices on arbitrary substrates by integrating multiple materials for significantly low-cost applications, including computing, energy conversion, data storage, imaging, solid-state lighting and displays.

Acknowledgment

This work was supported by Turkish Scientific and Research Council (TUBITAK) under BIDEB-2219 program.

References

[1] S.P. Chang, C.Y. Lu, S.J. Chang, Y.Z. Chiou, C.L. Hsu, P.Y. Su, T.J. Hsueh, Jpn. J. Appl. Phys. 50 (2011), 01AJ05-01–01AJ05-03.
[2] R.I. Badran, A. Umar, S. Al-Heniti, A. Al-Hajry, T. Al-Harbi, J. Alloys Compd. 508 (2010) 375–379.
[3] C. Klingshirn, Phys. Status Solidi (b) 244 (2007) 3027–3073.
[4] K. Sun, W. Wei, Y. Ding, Y. Jing, Z.L. Wang, D.L. Wang, Chem. Commun. 47 (2011) 7776–7778.
[5] X.D. Wang, Y. Ding, Z. Li, J.H. Song, Z.L. Wang, J. Phys. Chem. C 113 (2009) 1791–1794.
[6] Z.L. Wang, X.L. Li, F.X. Jiang, B.Q. Tian, B.H. Lu, X.H. Xu, Rare Metal Mater. Eng. 37 (2008) 831–834.
[7] Q. Yang, W.H. Wang, S. Xu, Z.L. Wang, Nano Lett. 11 (2011) 4012–4017.
[8] P.D. Yang, M.H. Huang, S. Mao, H. Feick, H.Q. Yan, Y.Y. Wu, H. Kind, E. Weber, R. Russo, Science 292 (2001) 1897–1899.
[9] Y. Natsume, H. Sakata, Mater. Chem. Phys. 78 (2003) 170–176.
[10] J.M. Myoung, J.H. Choi, S.N. Das, K.J. Moon, J.P. Kar, Solid State Electron. 54 (2010) 1582–1585.
[11] M.-C. Jeong, B.-Y. Oh, M.-H. Ham, S.-W. Lee, J.-M. Myoung, Small 3 (2007) 568–572.
[12] H. Sun, et al., Nanotechnology 17 (2006) 2271–2274.
[13] A. Wadeasa, S. Beegum, S. Raja, O. Nur, M. Willander, Appl. Phys. A: Mater. Sci. Process. 95 (2009) 807–812.
[14] W.Y. Zhang, S. Zhong, L.J. Sun, Z.X. Fu, Chin. Phys. Lett. 25 (2008) 1829–1831.
[15] Y.P. Hsieh, H.Y. Chen, M.Z. Lin, S.C. Shiu, M. Hofmann, M.Y. Chern, X.T. Jia, Y.J. Yang, H.J. Chang, H.M. Huang, S.C. Tseng, L.C. Chen, K.H. Chen, C.F. Lin, C.T. Liang, Y.F. Chen, Nano Lett. 9 (2009) 1839–1843.
[16] A.A. Ibrahim, A. Ashour, J. Mater. Sci.: Mater. El. 17 (2006) 835–839.
[17] H. Lei, C.H. Liu, B.X. Lin, Z.X. Fu, Chin. Phys. Lett. 22 (2005) 185–187.
[18] X.P. Li, B.L. Zhang, X. Dong, Y.T. Zhang, X.C. Xia, W. Zhao, G.T. Du, J. Lumin. 129 (2009) 86–89.
[19] C.H. Liu, Y.L. Chen, B.X. Lin, J.J. Zhu, Z.X. Fu, C. Peng, Z. Yang, Chin. Phys. Lett. 18 (2001) 1108–1110.
[20] W.Y. Zhang, X.P. Wu, L.J. Sun, B.X. Lin, Z.X. Fu, Acta Phys. Sin.: Chem. Ed. 57 (2008) 4471–4475.
[21] Y.T. Zhang, G.T. Du, B.L. Zhang, Y.G. Cui, H.C. Zhu, Y.C. Chang, Semicond. Sci. Technol. 20 (2005) 1132–1135.
[22] M. Benhaliliba, C.E. Benouis, M.S. Aida, A.S. Juarez, F. Yakuphanoglu, A.T. Silver, J. Alloys Compd. 506 (2010) 548–553.
[23] J.S. Yi, J. Yoo, J. Lee, S. Kim, K. Yoon, I.J. Park, S.K. Dhungel, B. Karunagaran, D. Mangalaraj, Thin Solid Films 480 (2005) 213–217.
[24] M. Yoshino, W.W. Wenas, A. Yamada, M. Konagai, K. Takahashi, Jpn. J. Appl. Phys. 32 (1993) 726–730.
[25] M.Ginting, J.D. Leslie, Can. J. Phys. 12 (1998) 448–455.
[26] I.-J.P. Jinsoo Song, Kyung-Hoon Yoon, Woo-Yeong Cho, Koeng-Su Lim, J. Korean Phys. Soc. 29 (1996).
[27] J. Lee, R. Myers, T. Dear, C. Gensler, Chemical Mechanical Planarization: An Effective Microfabrication and Micromachining Technology for MEMS, SPIE, 2003.
[28] J.H. Lee, B.O. Park, Thin Solid Films 426 (2003) 94–99.
[29] E. Hosono, S. Fujihara, T. Kimura, J. Mater. Chem. 14 (2004) 881–886.
[30] W.P. Tai, Y.S. Kim, Appl. Surf. Sci. 253 (2007) 4911–4916.
[31] M.H. Aslan, A.Y. Oral, E. Mensur, A. Gul, E. Basaran, Sol. Energy Mater. Sol. Cell 82 (2004) 543–552.
[32] JCPDS (Joint Committee on Powder Diffraction Standards) Card No.: 89-7102.
[33] S.Y. Kuo, W.C. Chen, F.I. Lai, C.P. Cheng, H.C. Kuo, S.C. Wang, W.F. Hsieh, J. Cryst. Growth 287 (2006) 78–84.
[34] P. Nunes, A. Malik, B. Fernandes, E. Fortunato, P. Vilarinho, R. Martins, Vacuum 52 (1999) 45–49.
[35] S. Mondal, A.K. Raychaudhuri, Appl. Phys. Lett. 98 (2011).
[36] W.Y. Zhang, D.K. He, Z.Z. Liu, L.J. Sun, Z.X. Fu, Optoelectron. Adv. Mater. 4 (2010) 1651–1654.
[37] D. Basak, R. Ghosh, S. Fujihara, J. Appl. Phys. 96 (2004) 2689–2692.
[38] S. Maensiri, C. Masingboon, V. Promarak, S. Seraphin, Opt. Mater. 29 (2007) 1700–1705.
[39] S.J. Kwon, J.H. Park, J.G. Park, Phys. Rev. E 71 (2005).
[40] N.F. Mott, E.A. Davis, Electronic Processes in Non-Crystalline Materials, 2nd ed., Clarendon Press/Oxford University Press, Oxford/New York, 1979.
[41] T.K. Subramanyam, B.S. Naidu, S. Uthanna, Cryst. Res. Technol. 35 (2000) 1193–1202.
[42] B.E. Sernelius, K.F. Berggren, Z.C. Jin, I. Hamberg, C.G. Granqvist, Phys. Rev. B 37 (1988) 10244–10248.
[43] A. Di Trolio, E.M. Bauer, G. Scavia, C. Veroli, J. Appl. Phys. 105 (2009) 113109–113114.
[44] L. Shen, Z.Q. Ma, C. Shen, F. Li, B. He, F. Xu, Superlattices Microstruct. 48 (2010) 426–433.
[45] B.S. Naidu, P.P. Ramesh, O.M. Hussain, S. Uthanna, P.J. Reddy, Mater. Lett. 34 (1998) 217–221.
[46] J.H. He, C.H. Ho, Appl. Phys. Lett. 91 (2007) 233105–233107.
[47] H.C. Casey, J. Muth, S. Krishnankutty, J.M. Zavada, Appl. Phys. Lett. 68 (1996) 2867–2869.
[48] F. Chaabouni, M. Abaab, B. Rezig, Superlattices Microstruct. 39 (2006) 171–178.
[49] H. Bo, M.Z. Quan, X. Jing, Z. Lei, Z.N. Sheng, L. Feng, S. Cheng, S. Ling, Z.C. Yue, Y.Z. Shan, Y.Y. Ting, Mater. Sci. Semicond. Process. 12 (2009) 248–252.